Physics in Medicine & Biology

IPEM Institute of Physics and Engineering in Medicine

NOTE

Microbubbles as a scattering contrast agent for grating-based x-ray dark-field imaging

To cite this article: A Velroyen *et al* 2013 *Phys. Med. Biol.* **58** N37

Phys. Med. Biol. **58** (2013) N37–N46 doi:10.1088/0031-9155/58/4/N37

NOTE

Microbubbles as a scattering contrast agent for grating-based x-ray dark-field imaging

A Velroyen[1], M Bech[1,2], A Malecki[1], A Tapfer[1], A Yaroshenko[1], M Ingrisch[3], C C Cyran[3], S D Auweter[3], K Nikolaou[3], M Reiser[3] and F Pfeiffer[1]

[1] Department of Physics and Institute of Medical Engineering, Technische Universität München, James-Franck-Straße, D-85748 Garching, Germany
[2] Medical Radiation Physics, Lund University, Barngatan 2:1, SE-22185 Lund, Sweden
[3] Institute for Clinical Radiology, Ludwig-Maximilians-University Hospital Munich, Marchioninistraße 15, D-81377 München, Germany

E-mail: astrid.velroyen@tum.de and franz.pfeiffer@tum.de

Received 21 August 2012, in final form 12 November 2012
Published 1 February 2013
Online at stacks.iop.org/PMB/58/N37

Abstract

In clinically established—absorption-based—biomedical x-ray imaging, contrast agents with high atomic numbers (e.g. iodine) are commonly used for contrast enhancement. The development of novel x-ray contrast modalities such as phase contrast and dark-field contrast opens up the possible use of alternative contrast media in x-ray imaging. We investigate using ultrasound contrast agents, which unlike iodine-based contrast agents can also be administered to patients with renal impairment and thyroid dysfunction, for application with a recently developed novel x-ray dark-field imaging modality. To produce contrast from these microbubble-based contrast agents, our method exploits ultra-small-angle coherent x-ray scattering. Such scattering dark-field x-ray images can be obtained with a grating-based x-ray imaging setup, together with refraction-based differential phase-contrast and the conventional attenuation contrast images. In this work we specifically show that ultrasound contrast agents based on microbubbles can be used to produce strongly enhanced dark-field contrast, with superior contrast-to-noise ratio compared to the attenuation signal. We also demonstrate that this method works well with an x-ray tube-based setup and that the relative contrast gain even increases when the pixel size is increased from tenths of microns to clinically compatible detector resolutions about up to a millimetre.

S Online supplementary data available from stacks.iop.org/PMB/58/N37/mmedia

(Some figures may appear in colour only in the online journal)

1. Introduction

Conventional x-ray imaging techniques in medical applications are purely based on the physical effect of absorption of the rays in the tissue. Since absorption depends on the material density, the generated contrast is optimal for structures with large density differences, for example between bone and soft tissue. To increase the otherwise poor contrast within soft-tissue types that provide only slight density differences, the application of contrast media with high atomic numbers is common practice (Dawson 1996). For absorption-based x-ray imaging, iodine-based contrast agents (CAs) are commonly employed for contrast enhancement. Intravascular administration of relatively high concentrations and volumes in a short period of time is necessary to create sufficient contrast (Christiansen 2005). The downside is that side effects can occur: in rare cases, such contrast media can provoke serious adverse reactions such as skin rash, renal impairment, or anaphylactic reactions of the cardiovascular or respiratory system as well as serious hyperthyroidism (Morcos and Thomsen 2001).

Unlike iodine-based contrast media, microbubble-based, echo-enhancing CAs used in ultrasound imaging can be administered to patients with impaired renal function (Krix and Jenne 2007, Quaia 2007) and thyroid dysfunction. Side-effects are usually mild and unspecific, but the possibility of anaphylactic reactions exists as with any drug (Schneider *et al* 2011). The microbubbles consist of shells of lipid monolayers, protein, sugar, or polymer encapsulating air or inert gases, which are less soluble in water. This results in an increased stability of the CA in blood vessels (Dietrich 2008). They usually have a diameter of several micrometres, i.e. sizes comparable to erythrocytes, to be able to pass small capillaries (Lindner *et al* 2002). In ultrasound imaging, the compressibility and therefore high sensitivity to acoustic waves of the microspheres is exploited to yield a contrast-enhanced image (Morgan *et al* 2000). The diagnostic capabilities of microspheres are numerous: they are applied in imaging vascularization of tumours, echocardiography, brain perfusion, and investigations of various organs (Clark and Dittrich 2000, Rim *et al* 2001, Nielsen and Bang 2004, Forsberg *et al* 2007). In addition, targeted microbubbles allow for imaging of molecular and metabolic processes (Heppner and Lindner 2005).

Recently, applications of microbubbles in imaging techniques other than ultrasound have been reported (Kogan *et al* 2010). Regarding x-ray imaging, it was shown that microsphere CAs generate a strongly improved contrast in analyser-based diffraction enhanced imaging (DEI) at a synchrotron source (Arfelli *et al* 2010). Here, the contrast mechanism differs from the conventional absorption-enhancing iodine CAs. Instead, DEI exploits ultra-small-angle scattering of x-rays at the gas-to-shell interfaces of the microbubbles, which lead to a deviation from the originally straight x-ray path direction. Consequently, contrast can be generated between x-ray scattering and non-scattering areas in the sample (Arfelli *et al* 2010), in addition to the extraction of absorption and refraction information (Chapman *et al* 1997). Furthermore, microbubbles have shown increased contrast in propagation-based phase-contrast imaging at a synchrotron source (Tang *et al* 2011).

X-ray phase-contrast and dark-field imaging based on Talbot–Lau interferometry exploit the same physical mechanism, i.e. the scattering and refraction of x-rays, but use a different experimental approach to extract the signal (Momose *et al* 2003, Weitkamp *et al* 2005, Pfeiffer *et al* 2006, 2008). Talbot–Lau interferometry utilizes a combination of microstructure gratings to extract three different, complementary signals: in addition to the conventional absorption-based signal, the phase shift that x-rays undergo when passing through matter as well as the local scattering power of the sample are measured simultaneously and are commonly called ‘differential phase contrast’ and ‘dark-field scattering contrast’, respectively.

The grating-based method is applicable at polychromatic laboratory x-ray sources without the necessity of a monochromator (Pfeiffer *et al* 2006, 2008), enabling the use of relatively high flux and short exposure times. Also cone-beam geometry, which is the usual case in clinical x-ray setups, does not pose a problem to the method. Therefore, Talbot–Lau interferometry has a high potential for future translation into a clinical environment. Recent studies have shown excellent results using the grating-based approach on imaging of biomedical samples in phase contrast (Pfeiffer *et al* 2007, Bech *et al* 2009, Donath *et al* 2010, Stampanoni *et al* 2011, Stutman *et al* 2011), as well as dark-field contrast (Ando *et al* 2005, Wen *et al* 2009, Potdevin *et al* 2012).

In this work, we show that microbubble-based ultrasound CAs can be used as dedicated CAs for x-ray dark-field imaging using Talbot–Lau interferometry. Furthermore, we prove the feasibility of dark-field contrast enhancement with a pixel size in the range of those of clinical x-ray scanners.

2. Materials and methods

2.1. Microbubble contrast agents and sample preparation

In this study, the x-ray scattering characteristics of three second-generation ultrasound microbubble CAs were investigated.

SonoVue® (by Bracco Imaging S.p.A., 10010 (TO), Italy) is a suspension of microbubbles consisting of a phospholipid shell filled with stabilized sulfur hexafluoride. After reconstitution of the agent by adding 0.9% saline solution to the powder-like lyophilisate, the concentration was 8 μl powder per ml contrast medium, providing a bubble concentration of up to 5×10^8 per ml (Schneider 1999). The mean diameter of the microbubbles is 2.5 μm with more than 90% smaller than 8 μm (Schneider 1999).

Vevo MicroMarker™ (manufactured by Bracco Imaging, sold by VisualSonics, Amsterdam, Netherlands) is a microbubble CA of similar constitution as SonoVue, with the shell made up of phospholipids. The bubbles contain a mixture of nitrogen and perfluorobutane gas. The freeze-dried powder in the vial was reconstituted by adding 0.7 ml of 0.9% saline solution. This way, a microbubble concentration of approximately 2.9×10^9 per ml was obtained. The median diameter in volume of these microbubbles is 2.3–2.9 μm.

Optison™ (by GE Healthcare AS, Oslo, Norway) is a suspension of microspheres consisting of human serum albumin, filled with the inert gas perflutren. The average amount of gas is 0.19 mg per ml CA; one millilitre contains $5–8 \times 10^8$ protein-type-A microspheres with a mean diameter of 3.0–4.5 μm, a maximum diameter of 32 μm and 95% of them being smaller than 10 μm. No reconstitution of the CA was necessary: by gentle mixing, the microbubbles were re-suspended to form an opaque, white liquid.

If no flow or agitation was applied to the re-suspended CAs, bubbles accumulated at the air-liquid interface within a few seconds. To avoid this non-physiological accumulation of contrast in one distinct area, samples of CA fixated in gelatin were prepared. For this purpose, 5 g of gelatin from porcine skin (Type A, Sigma-Aldrich Chemie GmbH, Steinheim, Germany) were dissolved in 100 ml desalted water during constant boiling, until a solution of about 40 ml was left. The gelatin mixture was allowed to cool down to approximately 40 °C under permanent stirring. 0.5 ml of each of the three CAs, which have been reconstituted or re-suspended at room temperature as described above, were distributed to 1.5 ml plastic centrifuge vials and gently heated in a water bath to 37 °C. Finally, 0.5 ml of the gelatin solution was added to each vial. The liquid in the vial was then gently sucked in and extruded from the pipette several times to gain a homogeneously mixed CA gelatin solution and to

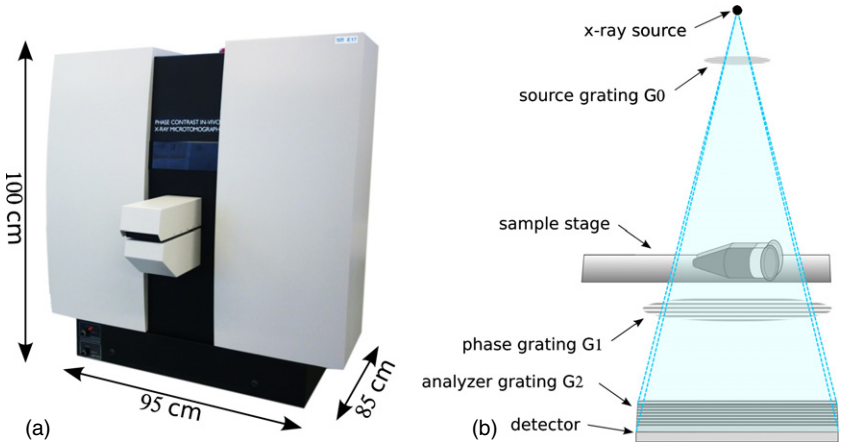

Figure 1. (a) Prototype preclinical phase-contrast and dark-field imaging CT scanner, described in detail in Tapfer *et al* (2011, 2012). (b) Schematic drawing of the setup including three-grating interferometer, x-ray tube source, detector and sample stage.

re-suspend accumulated microbubbles. Afterwards, the vials were cooled down quickly in an icy water bath to avoid de-mixing or re-accumulation of the microbubbles and to encourage fast hardening of the gelatin. Desalted water instead of the CA was used to create a reference sample.

2.2. Setup and image acquisition

The experiments were performed at a prototype preclinical phase-contrast and dark-field imaging CT scanner (fabricated by *Bruker microCT*, Kontich, Belgium; see figure 1(a)) previously described in Tapfer *et al* (2011, 2012). In the scanner, the experimental setup consisting of x-ray source, Talbot–Lau interferometer and detector (depicted schematically in figure 1(b)) is installed on a mechanical gantry that can be rotated around the sample stage. This feature, together with appropriate facilities for monitoring of breathing, temperature, and heartbeat, allows for *in vivo* absorption, phase and dark-field imaging of small rodents.

The x-ray source is a mini-focus tungsten x-ray tube (RTW, MCBM 65B-50 W) with a focal spot size diameter of approximately 50 μm. The images are recorded with a flatpanel detector (Hamamatsu C9312SK-06) with 2496 $\times$ 2304 pixels and 50 μm square pixel size. The setup has a source-to-sample and sample-to-detector distance of approximately 270 and 200 mm, respectively, resulting in a cone-beam geometry and an effective pixel size of 29 μm. The field of view at sample position is approximately 3.5 $\times$ 2.5 cm^2. The Talbot–Lau interferometer consists of three gratings (fabricated by *microworks*, Karlsruhe, Germany) with parameters optimized for a design energy of 23 keV. The heights and periods of the grating structures were 35 and 10 μm for the source grating G0, 4.0 and 3.2 μm for the phase grating G1, and 25 and 4.8 μm for the analyser grating G2, respectively. Source and analyser grating were made of gold, whereas the phase grating consisted of nickel structures. The source grating was positioned 31 mm from the x-ray tube. G0 and G1 are 300 mm apart, whereas G1 and G2 have a distance of 145 mm, which corresponds to the first fractional Talbot distance.

To acquire absorption, phase contrast and dark-field images, phase stepping, as described for example in Weitkamp *et al* (2005) and Pfeiffer *et al* (2008), was applied, using ten phase

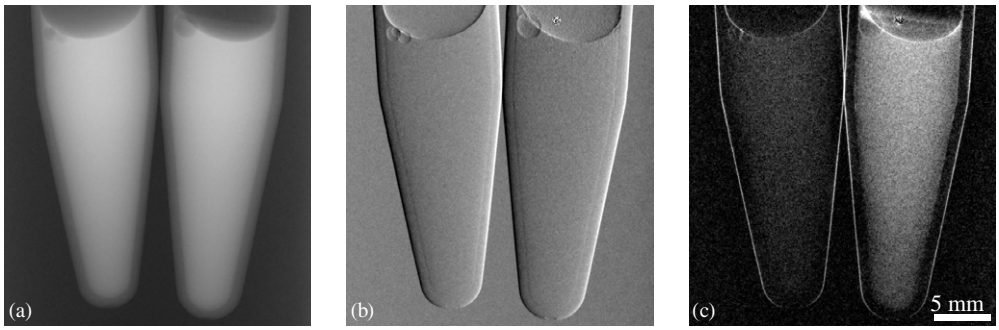

Figure 2. Microsphere-based CA Optison fixed in gelatin (right container) versus reference sample (water in gelatin, left container), imaged in three different modalities with the range of the grey values given in brackets. (a) Conventional absorption-based image [0, 0.6], (b) differential phase-contrast image [−0.6, 0.6], (c) dark-field contrast image [0, 0.4].

steps. Images were taken at a source voltage of approximately 30 kVp and with an exposure time of 10 s per step, i.e. a total exposure of 100 s to create one set of images of the three modalities. The processed images cover a detector area of 930 × 970 pixels.

2.3. Data analysis

To obtain a quantitative measure for the contrast in the images of the three different microbubble CAs, the contrast-to-noise ratio (CNR) of the absorption-based and dark-field images was calculated as

$$\mathrm{CNR} = \frac{|S_{\mathrm{CA}} - S_{\mathrm{Ref}}|}{\sigma_{\mathrm{Ref}}}. \tag{1}$$

S_{CA} and S_{Ref} denote the mean of the absorption or dark-field signal in a certain region of interest (ROI) in the CA sample and the reference (Ref) sample, respectively. The regions of interests were manually chosen areas of 64 × 64 pixels in the centre of the cylindrical part of the vials, just like those depicted in case of the Optison sample by the blue boxes in figure 4(a). σ_{Ref} represents the standard deviation of the according signal in the ROI of the reference sample, as a measure for noise in the image.

To demonstrate the feasibility of the application of dark-field contrast enhancement in setups with potentially larger pixel size, a series of binned images of the Optison measurement was created, using 2 × 2, 4 × 4, 8 × 8, 16 × 16, and 32 × 32 binning of the raw image data, before extracting the absorption-based and dark-field image from the raw stepping scan data. The ROI size was adapted accordingly to cover the same physical region. The same CNR analysis as described above was then applied to the binned images.

3. Results and Discussion

Figure 2 displays the Optison sample next to the reference sample imaged in three different contrast modalities. The conventional absorption-based projection image in figure 2(a) shows no significant contrast enhancement between the reference and the CA sample, because the microbubbles mainly consist of elements with low atomic numbers. The differential phase-contrast image (figure 2(b)) enhances the edges of the sample containers as the features that strongly refract the x-ray wave-front passing through the sample. On the contrary, the

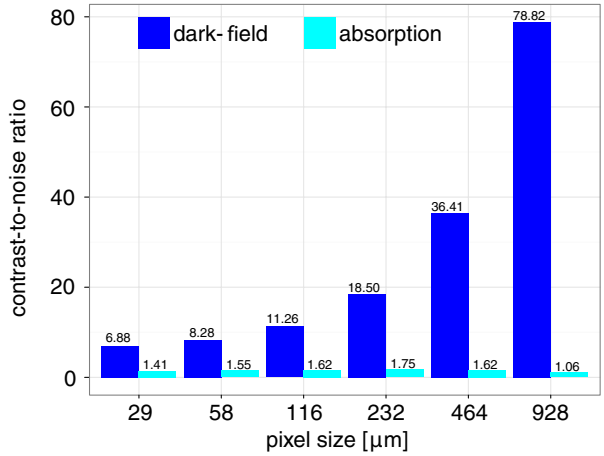

Figure 3. Bar plot of the CNR in comparison for dark-field and absorption image at different binning stages for the Optison sample. The CNR was calculated in a ROI of 64 × 64 pixels of the unbinned case, down to 2 × 2 pixels in the 32-fold-binning case.

scattering-based dark-field image in figure 2(c) shows a clearly enhanced signal in the right vial containing the Optison CA, due to x-ray scattering at the interfaces between the gas and the shell of the bubbles. Thus, we conclude that there is great potential for the use of microbubble-based ultrasound contrast media as dedicated x-ray dark-field CAs.

Figure 3 shows the resulting CNR values of dark-field and absorption-based images for the binning series of the Optison sample measurement at 30 kVp. The values clearly indicate that the dark-field signal gains much more from the noise reduction due to binning than the absorption signal, since the CNR of the dark-field signal increases from 6.88 to 78.82 in the binning series up to 32-fold binning. The CNR of the absorption signal only rises slightly from 1.41 to 1.75 for the binning series up to 8-fold binning. For the 16- and 32-fold binning case, the dark-field CNR is still increasing, whereas the absorption CNR drops to 1.62 and 1.06. This phenomenon could be caused by low statistics, since for example the ROI in the 32-fold binning case only consists of 2 by 2 pixels. Taken as a whole, the binning series demonstrates clearly the ability of the dark-field signal to image microstructures with sub-pixel sizes (Chen *et al* 2010, Bech *et al* 2010). The noise reduction and contrast gain in the dark-field images is clearly visible in figure 4(a)–(c), which shows the unbinned image in comparison with the 4 × 4 and the 16 × 16 binned image of the Optison sample.

Unexpectedly, not all CA samples provide an equally strong x-ray dark-field signal enhancement. Table 1 lists the raw signal values in the ROI as well as the CNR values calculated from the dark-field and absorption signals for each of the three CAs, for the unbinned case. Unlike the contrast behaviour of the Optison sample, the CNR of SonoVue and Vevo MicroMarker are not significantly different regarding dark-field and absorption.

The reason for this different behaviour of the Optison sample compared to the SonoVue and Vevo MicroMarker samples is not clear. The dark-field contrast sensitivity for different microstructure particles is dependent on the imaging-system parameters (Lynch *et al* 2011) and thus varies for different bubble sizes in one system. Since the exact bubble-size distributions of each tested CA brand is unknown to the authors except for SonoVue (Schneider *et al* 1995), it cannot be stated whether or not these differ significantly such that they could cause the strong difference in contrast enhancement. To investigate the bubble-size dependence more generally,

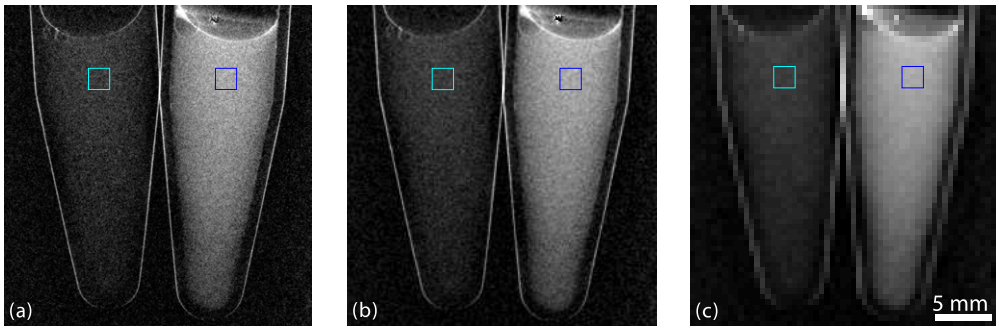

Figure 4. Dark-field images of the reference (left container) and Optison sample (right container) in three different binning stages: (a) 1 × 1 pixels, (b) 4 × 4 pixels, (c) 16 × 16 pixels. The blue boxes indicate the regions of interest in which the CNR was calculated (see figure 3). The greyscale range is [0, 0.4].

Table 1. Signal strength of CA sample (S_{CA}) and reference sample (S_{Ref}) and standard deviation (σ_{Ref}) of reference sample as a measure for noise, for dark-field and absorption image in comparison for different CAs. The CNR was calculated from these values taken from regions of interest of 64 × 64 pixels in the centre of the cylindrical part of the centrifuge vials.

		S_{CA}	S_{Ref}	σ_{Ref}	CNR
SonoVue	Dark-field	0.898	0.933	0.027	0.54
	Absorption	0.157	0.524	0.005	0.48
Vevo MicroMarker	Dark-field	0.889	0.905	0.029	1.32
	Absorption	0.540	0.538	0.003	1.54
Optison	Dark-field	0.735	0.904	0.025	6.88
	Absorption	0.547	0.542	0.004	1.41

a small simulation study of gas-filled spheres in water, similar to those presented in Malecki *et al* (2012), was performed with parameters adapted to the geometry and the interferometric components of the experimental setup used in this work. The sphere diameter was identical for all spheres in every single simulated volume. In between the volumes the diameter and the number of spheres was varied, while keeping the volume fraction occupied by the gas constant. The variation of the diameter revealed an optimal dark-field contrast sensitivity at diameters between 2 and 5 μm, as can be seen in figure 5. Thus, the mean bubble sizes of the tested microbubble brands already comply well with the optimal diameter.

The CA inherent difference in the shell constitution of the microbubbles is assumed not to cause such large variations in dark-field contrast level, because the refractive index change between gas and the surrounding medium (i.e. water and gelatine) possibly dominates over a comparatively thin and thus negligible lipid or protein shell or diminutive variations of the refractive index of different gas fillings. Since SonoVue and Vevo MicroMarker shells consist of phospholipids, whereas the Optison shell is based on human serum albumin, the question can be posed whether the phospholipid shell does not properly form in the *in vitro* situation. Because this case cannot be ruled out completely, it is of high importance to test the potential dark-field CAs in the situation for which they were designed and in which they would stay intact: the *in vivo* situation. *In vivo*, the requirement of flow and turbulence to avoid accumulation of bubbles is fulfilled, without any potential changes of the microbubbles because of an unphysiological environment. To exclude that the process of gelatin-mixing

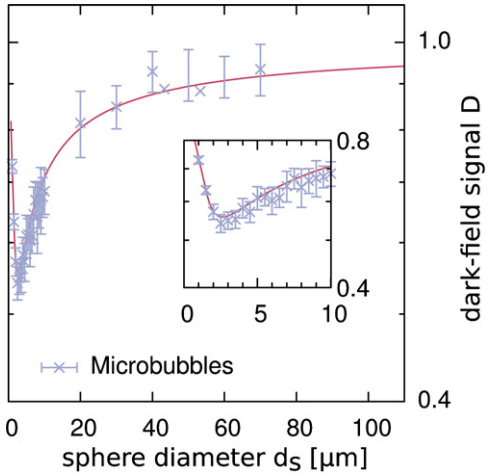

Figure 5. Simulated dependence of the dark-field signal D on the diameter d_s of the microbubbles. The simulations were carried out according to Malecki *et al* (2012) with a point source to create a cone beam as in the experiment. The total volume fraction of the gas distributed on the equally sized spheres was kept constant. From left to right the sphere diameter increases from 1 μm up to 10 μm in steps of 0.5 μm and from 10 μm up to 75 μm in steps of 5 μm. The number of spheres changes accordingly. To visualize the details in the region of maximum sensitivity the inset shows a magnification of the results below 10 μm. The red line shows the theoretical value according to Lynch *et al* (2011), modified by a magnification factor that takes the cone-beam geometry into account.

and hardening affected the CA brands differently, a control measurement with the pure, non-fixated, and—to avoid any possible reason for destruction—very gently reconstituted CAs was performed, hazarding the consequence of bubble accumulation. This measurement only confirmed the result obtained with the gelatin-fixated samples: Optison showed a much more enhanced dark-field contrast than SonoVue and Vevo MicroMarker, although the accumulation of bubbles appeared similar to the naked eye (see supplementary information figure 1, available from stacks.iop.org/PMB/58/N37/mmedia).

Another finding to be pointed out is that the inability of the Vevo MicroMarker to generate enhanced dark-field contrast on the contrary to Optison cannot even be overcome by its concentration that is one order of magnitude higher than the bubble concentration of Optison.

The contrast strength of the microbubble CA depends on different parameters: the dark-field signal strength scales with the number of bubbles (or shell-gas-interfaces) in the beam path. Therefore, the bubble concentration in the CA as well as the sample thickness contribute to the signal strength in a dark-field radiography image. This implies that an *in vitro* simulation of the signal to be expected *in vivo* is challenging due to varying blood vessel or lumen size in the animal, as well as the dynamic intermixture of blood and CA resulting in locally different concentrations. These open questions, as well as the influence of the structures present in a living animal that contribute to a background signal, can only be reasonably approached by actual proof-of-principle *in vivo* measurements. Besides these environmental dependencies of the contrast behaviour, it also depends on the grating pitch and x-ray energy, i.e. the design of the grating interferometer.

The objective of this work was to show the feasibility of using microbubble-based ultrasound CAs as a contrast medium for x-ray dark-field imaging. Future experiments have to identify the optimal microbubble CA for x-ray dark-field imaging, concerning stability,

bubble size and concentration. Also, a pharmacological re-design of existing microbubble CAs specifically for dark-field imaging should be considered regarding the optimization of parameters like concentration or microbubble size within the limits of pharmacological safety and tolerance. Furthermore, the acquisition protocol for contrast enhanced dark-field projections needs to be optimized in terms of time and dose reduction, which was not the scope of this study.

Further investigations might allow new clinical applications such as multimodal ultrasound and x-ray imaging, for example in angiography, as well as a diagnostic alternative to the administration of iodine-based CAs, once dark-field imaging is clinically established.

4. Summary

Although iodine-based x-ray CAs have been improved in recent years, they still have a non-negligible toxicity, especially for patients with renal impairment. The need for less-invasive techniques to enhance soft-tissue contrast supports the use of alternative imaging modalities such as dark-field and phase-contrast imaging as well as the examination of alternative CAs, such as microbubble-based ultrasound contrast media. Based on the images shown in this work, we conclude that such microbubble CAs can be successfully employed to create contrast-enhanced dark-field images that are acquired using a Talbot–Lau interferometer. The proved feasibility of microbubble-based dark-field contrast enhancement with large pixel sizes, together with the large potential of the implementation of Talbot–Lau interferometry into a clinical environment, strongly promote the use of microbubbles as a dedicated dark-field x-ray CA. This has, so far, only been shown at analyser-based setups with synchrotron radiation. To optimize the contrast behaviour, which depends on various parameters of the CA and the setup, further studies must be conducted, including *in vivo* tests that provide the environment for which the microbubble substances have been developed for.

Acknowledgments

We acknowledge financial support through the DFG Cluster of Excellence Munich-Centre for Advanced Photonics (MAP, grant no. DFG EXC-158), the DFG Gottfried Wilhelm Leibniz program and the European Research Council (ERC, FP7, StG 240142). We thank Katrin Suppelt, Visualsonics, for providing the Vevo MicroMarker vials and for valuable advice on their handling. This work was carried out with the support of the Karlsruhe Nano Micro Facility (KNMF, www.kit.edu/knmf), a Helmholtz Research Infrastructure at Karlsruhe Institute of Technology (KIT, www.kit.edu). We acknowledge Bruker microCT for technical support. AV, AM, AT and AY acknowledge the TUM Graduate School for the support of their studies.

References

Ando M *et al* 2005 Attempt at visualizing breast cancer with x-ray dark field imaging *Japan. J. Appl. Phys.* **44** L528–31

Arfelli F, Rigon L and Menk R H 2010 Microbubbles as x-ray scattering contrast agents using analyzer-based imaging *Phys. Med. Biol.* **55** 1643–58

Bech M, Bunk O, Donath T, Feidenhans'l R, David C and Pfeiffer F 2010 Quantitative x-ray dark-field computed tomography *Phys. Med. Biol.* **55** 5529–39

Bech M, Jensen T H, Feidenhans'l R, Bunk O, David C and Pfeiffer F 2009 Soft-tissue phase-contrast tomography with an x-ray tube source *Phys. Med. Biol.* **54** 2747–53

Chapman D, Thomlinson W, Johnston R E, Washburn D, Pisano E, Gmür N, Zhong Z, Menk R, Arfelli F and Sayers D 1997 Diffraction enhanced x-ray imaging *Phys. Med. Biol.* **42** 2015–25

Chen G H, Bevins N, Zambelli J and Qi Z 2010 Small-angle scattering computed tomography (SAS-CT) using a Talbot-Lau interferometer and a rotating anode x-ray tube: theory and experiments *Opt. Express* **18** 12960–70

Christiansen C 2005 X-ray contrast media–an overview *Toxicology* **209** 185–7
Clark L N and Dittrich H C 2000 Cardiac imaging using optison *Am. J. Cardiol.* **86** 14–8
Dawson P 1996 X-ray contrast-enhancing agents *Eur. J. Radiol.* **23** 172–7
Dietrich C F 2008 *Endosonographie: Lehrbuch und Atlas des endoskopischen Ultraschalls* (Stuttgart: Georg Thieme Verlag KG)
Donath T, Pfeiffer F, Bunk O, Grünzweig C, Hempel E, Popescu S, Vock P and David C 2010 Toward clinical x-ray phase-contrast CT: demonstration of enhanced soft-tissue contrast in human specimen *Invest. Radiol.* **45** 445–52
Forsberg F, Piccoli C W, Merton D A, Palazzo J J and Hall A L 2007 Breast lesions: imaging with contrast-enhanced subharmonic US–initial experience *Radiology* **244** 718–26
Heppner P and Lindner J R 2005 Contrast ultrasound assessment of angiogenesis by perfusion and molecular imaging *Expert Rev. Mol. Diagn.* **5** 447–55
Kogan P, Gessner R and Dayton P A 2010 Microbubbles in imaging: applications beyond ultrasound *Bubble Sci. Eng. Technol.* **2** 3–8
Krix M and Jenne J W 2007 Ultrasound contrast agents. Pharmaceutical drug safety and bioeffects *Der Radiologe* **47** 800–7
Lindner J R, Song J, Jayaweera A R, Sklenar J and Kaul S 2002 Microvascular rheology of Definity microbubbles after intra-arterial and intravenous administration *J. Am. Soc. Echocardiogr.* **15** 396–403
Lynch S K, Pai V, Auxier J, Stein A F, Bennett E E, Kemble C K, Xiao X, Lee W K, Morgan N Y and Wen H H 2011 Interpretation of dark-field contrast and particle-size selectivity in grating interferometers *Appl. Opt.* **50** 4310–9
Malecki A, Potdevin G and Pfeiffer F 2012 Quantitative wave-optical numerical analysis of the dark-field signal in grating-based x-ray interferometry *EPL* **99** 48001
Momose A, Kawamoto S, Koyama I, Hamaishi Y, Takai K and Suzuki Y 2003 Demonstration of X-ray Talbot interferometry *Japan. J. Appl. Phys.* **42** L866–8
Morcos S and Thomsen H 2001 Adverse reactions to iodinated contrast media *Eur. Radiol.* **11** 1267–75
Morgan K E, Allen J S, Dayton P a, Chomas J E, Klibaov a L and Ferrara K W 2000 Experimental and theoretical evaluation of microbubble behavior: effect of transmitted phase and bubble size *IEEE Trans. Ultrason., Ferroelectr. Freq. Control* **47** 1494–509
Nielsen M B and Bang N 2004 Contrast enhanced ultrasound in liver imaging *Eur. J. Radiol.* **51** (suppl) S3–8
Pfeiffer F, Bech M, Bunk O, Kraft P, Eikenberry E F, Brönnimann C, Grünzweig C and David C 2008 Hard-X-ray dark-field imaging using a grating interferometer *Nature Mater.* **7** 134–7
Pfeiffer F, Bunk O, David C, Bech M, Le Duc G, Bravin A and Cloetens P 2007 High-resolution brain tumor visualization using three-dimensional x-ray phase contrast tomography *Phys. Med. Biol.* **52** 6923–30
Pfeiffer F, Weitkamp T, Bunk O and David C 2006 Phase retrieval and differential phase-contrast imaging with low-brilliance X-ray sources *Nature Phys.* **2** 258–61
Potdevin G *et al* 2012 X-ray vector radiography for bone micro-architecture diagnostics *Phys. Med. Biol.* **57** 3451–61
Quaia E 2007 Microbubble ultrasound contrast agents: an update *Eur. Radiol.* **17** 1995–2008
Rim S J, Leong-Poi H, Lindner J R, Couture D, Ellegala D, Mason H, Durieux M, Kassel N F and Kaul S 2001 Quantification of Cerebral Perfusion With "Real-Time" Contrast-Enhanced Ultrasound *Circulation* **104** 2582–87
Schneider A, Johnson L, Goodwin M, Schelleman A and Bellomo R 2011 Bench-to-bedside review: contrast enhanced ultrasonography–a promising technique to assess renal perfusion in the ICU *Crit. Care* **15** 157
Schneider M 1999 SonoVue, a new ultrasound contrast agent *Eur. Radiol.* **9** (suppl 3) S347–8
Schneider M, Arditi M, Barrau M and Brochot J 1995 BR1: a new ultrasonographic contrast agent based on sulfur hexafluoride-filled microbubbles *Invest. Radiol.* **30** 451–7
Stampanoni M, Wang Z, Thüring T, David C, Roessl E, Trippel M, Kubik-Huch R A, Singer G, Hohl M K and Hauser N 2011 The first analysis and clinical evaluation of native breast tissue using differential phase-contrast mammography *Invest. Radiol.* **46** 801–6
Stutman D, Beck T J, Carrino J A and Bingham C O 2011 Talbot phase-contrast x-ray imaging for the small joints of the hand *Phys. Med. Biol.* **56** 5697–720
Tang R, Xi Y, Chai W M, Wang Y, Guan Y, Yang G Y, Xie H and Chen K M 2011 Microbubble-based synchrotron radiation phase contrast imaging: basic study and angiography applications *Phys. Med. Biol.* **56** 3503–12
Tapfer A, Bech M, Pauwels B, Liu X, Sasov A and Kenntner J 2011 *Med. Phys.* **38** 5910–5
Tapfer A *et al* 2012 *Proc. Nat. Acad. Sci. USA* **109** 15691–6
Weitkamp T, Diaz A, David C, Pfeiffer F, Stampanoni M, Cloetens P and Ziegler E 2005 X-ray phase imaging with a grating interferometer *Opt. Express* **13** 6296–304
Wen H, Bennett E E, Hegedus M M and Rapacchi S 2009 Fourier X-ray scattering radiography yields bone structural information *Radiology* **251** 910–8